# Semiclassical Approach to Few-Body Problems
## —*The Helium Atom*—

D. WINTGEN, A. BÜRGERS, K. RICHTER*) and G. TANNER

*Fakultät für Physik, Universität Freiburg*
*Hermann-Herder-Str. 3, D-79104 Freiburg, Germany*

We report on recent progress in the semiclassical description of two-electron atoms. We show that the classical dynamics for the helium atom is of mixed phase space structure, i.e. regular and chaotic motion coexists. Semiclassically, both types of motion require separate treatment. Stability islands are quantized via the Einstein-Brillouin-Keller torus-quantization procedure, whereas a periodic-orbit cycle expansion approach accounts for the states associated with hyperbolic electron pair motion. The results are compared with highly accurate *ab initio* quantum calculations, some of which are reported here for the first time.

## § 1. Introduction

Semiclassical methods for systems of few degrees $d$ of freedom (typically $d=1$) are well established and widely applied.[1),2)] However, the failure of the old quantum theory to give a reasonable estimate for the ground-state energy of the helium atom (see, e.g., the old review by Van Vleck[3)]) and of the $H_2^+$-molecule[4)] retained a pessimistic view concerning a semiclassical treatment of few-body systems with several degrees of freedom.

The failure of the old quantum theory is not an intrinsic defect of the theory as conjectured by Born.[5)] At least two ingredients were not fully developed at the early days of the Copenhagen School: The Maslov indices related to conjugated points along classical trajectories and their importance for the approach to wave mechanics (which was not developed at those times) were not properly accounted for, and the precise role of periodic trajectories when the classical dynamics are non-integrable or even chaotic was unknown.

The pessimistic point of view dominated the research for several decades and there were no serious (and successful) attempts to attack the problem until Leopold and Percival[6)] in 1980 gave a reasonable estimate of the ground-state energy of the helium atom using semi-classical perturbation theory. A proper treatment of the helium atom is still an outstanding problem of the semiclassical theory. The helium atom therefore remains the essential touch-stone of semiclassical mechanics, even though considerable progress in the development of the formal theory has been achieved within the last years, parts of which are reviewed herein.

A semiclassical description of two-electron atoms is also highly desirable, because most parts of the spectral regions are still unexplored, both experimentally

*) Present address: Division de Physique Théorique, Institut de Physique Nucléaire, 91406 Orsay, France.

and quantum theoretically. From a conceptual point of view highly accurate quantum calculations are not too difficult to perform. However, the high dimensionality of the problem combined with the vast density of states makes the calculations cumbersome and elaborate. In addition, one has to deal with singular potentials, long-ranged interactions, and many open decay-channels, all of which prevents the success of brute-force methods. Furthermore, the problem of *understanding the structure* of the quantum solutions still remains after solving the Schrödinger equation. Again, the simple interpretation of classical and semiclassical methods assists in illuminating the structure of the solutions. Classical calculations may also help to uncover local integrals of motions or adiabatic coordinates. Exploiting such properties may facilitate (approximate) quantum calculations considerably.

The necessary ingredient for any semiclassical analysis is a proper understanding of the underlying classical dynamics. Unfortunately, this information is highly non-trivial to obtain. The equations of motion are multi-dimensional, non-integrable and singular, hence anything but an easy-to-do-job. In addition, the independent particle case $1/Z=0$ ($Z$ is the nuclear charge) is highly degenerate, which prohibits an application of the KAM theory to derive an independent particle limit. In other words, the phase space structure of the hydrogenic motion of two independent electrons depends on an (infinitesimal) perturbation and not only on the zero-order Hamiltonian itself. As a matter of fact, it was only recently shown that the motion of two-electron atoms is not ergodic.[7]

In this contribution we review on recent progress in the classical and semiclassical description of two-electron atoms. We show that the classical phase space is of mixed structure, i.e., regular and irregular motion of the electron pair co-exist. Roughly, the angular type of motion (i.e., bending motion of the electron pair relative to the nucleus) is mostly stable, whereas radial motion is mostly (but not always) unstable. The radial instability typically leads to ionization of one electron (we restrict the analysis to energies below the three-particle breakup threshold). A semiclassical treatment has to distinguish between fully stable (i.e., stable in all dimensions) and (partly) unstable motion. Fully stable motion allows for torus quantization, and this applies to the electron pair motion, where both electrons are located on the same side of the nucleus in a near-collinear configuration. The classical motion for near-collinear configurations with both electrons on different sides of the nucleus turns out to be fully chaotic. In this case the semiclassical Gutzwiller theory combined with the cycle expansion method yields good results.

Our main concern lies in demonstrating the power of semiclassical methods for two-electron atoms and how the semiclassical results compare with highly accurate quantum results, but the methods apply to few body systems quite generally. In § 2 we will describe the classical motion of the electron pair in helium. We particularly focus to motion in the symmetry planes of the problem. A method to obtain highly accurate quantum results for the problem is briefly described in § 3. We use semiclassical mechanics to quantize the motion in the symmetry planes in § 4. The motion off the symmetry planes is consistently taken into account by linearizing the motion.

We focus on collinear motion where the electrons are either on the same side or on different sides of the nucleus. This maximizes or minimizes the electron-electron

repulsion and these configurations describe the energetically unfavoured and favoured quantum states of the problem.

## § 2. Classical motion in helium

There are only few rigorous results about the general classical three-body Coulomb problem. The reason for the lack of popularity of quantitative classical studies is obvious: the equations of motion are multi-dimensional, non-integrable, and singular. In addition, the independent particle case $1/Z=0$ ($Z$ is the nuclear charge) is highly degenerate, which prohibits a direct application of the KAM theorem to derive a proper independent particle limit. Recent quantitative analyses of the problem can be found in Refs. 7)~15).

An essential ingredient for the classical analysis of the three-body Coulomb problem is the regularization of the equations of motion.[16] For a nucleus with charge $Z$ and infinite mass the Hamiltonian reads (atomic units used, $e=m_e=1$):

$$H=\frac{\boldsymbol{p}_1^2+\boldsymbol{p}_2^2}{2}-\frac{Z}{r_1}-\frac{Z}{r_2}+\frac{1}{r_{12}}. \tag{1}$$

The electron-nucleus distances are given by $r_i$, $i=1, 2$, and the distance between the electrons is $r_{12}$. Whenever an inter-particle distance vanishes (particle collision) the potential energy diverges. There is a striking difference in the topology of the various collisions. In analogy to the motion of the electron in the hydrogen atom, the motion can be regularized for *binary collisions*, where only one inter-particle distance vanishes. However, the *triple collision* $r_1=r_2=r_{12}=0$ cannot be regularized, i.e., these solutions have branch points of infinite order.[17] As a consequence there is a continuous family of trajectories coming out of the triple collision. A numerically convenient method to regularize the binary collisions can be found in Refs. 7) and 15).

The energy $E$ and the total angular momentum $\boldsymbol{L}$ are constants of motion. Furthermore, the Hamiltonian (1) is invariant under reflection $(\boldsymbol{r}_1, \boldsymbol{r}_2)\to(-\boldsymbol{r}_1, -\boldsymbol{r}_2)$ and particle exchange $(\boldsymbol{r}_1, \boldsymbol{r}_2)\to(\boldsymbol{r}_2, \boldsymbol{r}_1)$. The potential appearing in (1) is homogeneous in coordinates and momenta and the equations of motion can be scaled to energy independent form. The accumulated action along a classical path is then $\tilde{S}(E)=2\pi z S$ with $z=(-E)^{-1/2}$ and $2\pi S$ the action at energy $E=-1$.

Here we shall focus on total angular momentum $\boldsymbol{L}=0$, for which the motion of the electrons is confined to a space fixed plane in configuration space. This removes three of the total of six degrees of freedom, and we take the three inter-particle distances $r_i$ as dynamical variables. It is convenient to replace these by the *perimetric coordinates*[18]

$$x=r_1+r_2-r_{12}, \quad y=r_1-r_2+r_{12}, \quad z=-r_1+r_2+r_{12} \tag{2}$$

with $x, y, z\geq 0$. The perimetric coordinates treat all inter-particle distances democratically. The discrete symmetries of the Hamiltonian (1) are readily identified as invariant planes in the perimetric coordinate set. Collinear motion with both electrons on different sides of the nucleus is confined to the $x\equiv 0$ plane. Collinear motion with both electrons localized on the same side of the nucleus is given by either $y\equiv 0$

or $z\equiv 0$. Finally, motion on the so-called *Wannier ridge*[19] $r_1\equiv r_2$ takes place in the $y\equiv z$ plane. The electron motion in the invariant planes becomes essentially two-dimensional. The third degree of freedom is in a static equilibrium and taken into account by linearizing the equations of motion around the symmetry plane.

Here we will focus on near-collinear configurations only, but as we will see this is already enough to uncover the variety of the problem and to draw some definitive conclusions about the full problem. Our main concern is to unravel the structure and the organization of the periodic orbits. They are the main ingredients of modern multi-dimensional semiclassical theories as discussed in the next sections. The radial motion along the Wannier ridge of symmetrical electron configurations $r_1\equiv r_2$ is (except for the so-called Langmuir orbit[7]) extremely unstable and of minor importance for a semiclassical treatment. It may be important, however, to understand the transition region of configurations beyond the states dominated by collinear motion.

### A. *The $Z^{2+}e^-e^-$ configuration*

Consider a collinear arrangement of a nucleus of charge $Z$ and of two electrons, both being on the same side of the nucleus. The fundamental periodic motion of such a configuration is a coherent oscillation of both electrons with the same frequency but, as it turns out, with large differences in their individual radial amplitudes and velocities as shown in Fig. 1(a) for helium ($Z=2$). The outer electron appears to stay nearly frozen at some fixed radial distance. For this reason we label the orbits as *frozen planet configurations*. The minimal nuclear charge to bind an electron pair in this type of collinear configuration is $Z>1$; otherwise the outer electron potential is purely repulsive. On the other hand the inter-electron interaction prevents the electrons to pass each other, i.e., $1/Z$ must be non-zero for these states: The repulsive inter-electron interaction is of crucial importance for the formation of these states. Thus the configurations considered here cannot be described within an independent particle model and are of highly non-perturbative nature. The degree of dynamical localization of the outer electron is mostly pronounced for helium and becomes weaker for larger integer values of $Z$.

Most remarkably, the periodic orbit (PO) of Fig. 1(a) is linearly stable with respect to variations in the initial conditions. This is demonstrated in Fig. 1(b) which shows the resulting (regular) motion of the electrons when they are initially in a slightly off-collinear arrangement. The inner electron moves on perturbed Kepler ellipses around the nucleus, while the outer electron remains trapped at large radial distances following the slow angular oscillations of the inner electron.

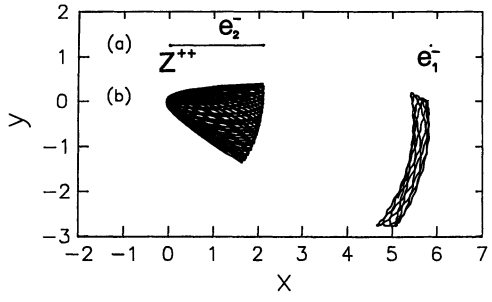


Fig. 1. (a) The straight line motion of the electron pair for the frozen planet periodic orbit, while a non-periodic but regular trajectory in its neighborhood is shown in (b). Energy scaled units $(-E)\boldsymbol{r}$ are used.

For collinear configurations the motion is confined to the three-

dimensional energy shell of a four-dimensional subspace of the full phase space. It is convenient to visualize the phase space structure by taking Poincaré surfaces of section. Such a section is shown for helium in Fig. 2. The phase space position $\{r_1, p_1\}$ of the outer electron is monitored each time the inner electron approaches the nucleus ($r_2=0$). The PO shown in Fig. 1(a) appears as the elliptic fixed point in the center of the extended torus structure. Near the fixed point the motion of the outer electron is nearly harmonic, but for large radial distances the tori are deformed according to the almost Keplerian motion of the outer electron. The non-closed manifolds surrounding the tori represent (regular) trajectories for which the outer electron ionizes with $p_1 \to (2E_1+2/r_1)^{1/2}$ ($E_1$ is the asymptotic excess energy of the ionizing electron). Recalling the additional stability of the bending degree of freedom (i.e., motion off the collinear arrangement), the fundamental PO of Fig. 1 is embedded in a fully six-dimensional island of stability in phase space.

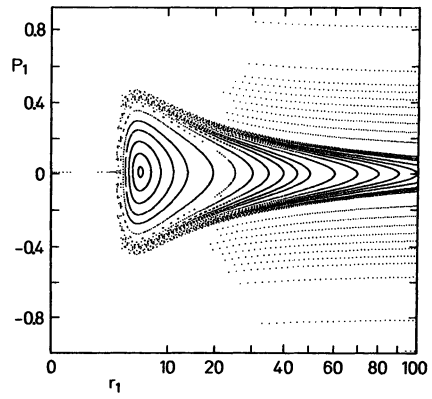


Fig. 2. Poincaré surface of section ($r_2=0$) for collinear configurations with both electrons on the same side of the nucleus ($E=-1$).

The near-integrability of the three-body Coulomb problem for asymmetric configurations as shown in Figs. 1, 2 is a remarkable fact, which nevertheless was unknown until recently. The stability of the outer electron with respect to radial motion can be understood in a static model (e.g., by fixing the inner electron at its classical expectation value or its outer classical turning point) but the stability with respect to the bending degree of freedom is somewhat surprising and its origin is purely dynamical. It is also unexpected and surprising that these classical configurations are extremely stable against autoionization, which is allowed energetically. Intuitively, one would expect that the inner electron 'kicks' the loosely bound outer electron out because the electron-electron interaction $1/r_{12}$ is maximized in such a collinear configuration. However, as we will see in the next section instabilities of the system emerge mostly from the (non-regularisable) triple collisions, where *all* inter-particle distances vanish.

It follows from the near-integrable nature of the frozen-planet configurations that *locally* the Hamiltonian (1) can be written to good approximation as a function of three action variables $J_1$, $J_2$, $J_3$,[4]

$$H(p_1, r_1, p_2, r_2, p_{12}, r_{12}) = H(J_1, J_2, J_3)\,. \tag{3}$$

The action variables measure the symplectic area enclosed by the different independent circuits around the tori to which the motion is confined. The main information on the classical motion is then contained in a single energy-surface $H(J_1, J_2, J_3)=\text{const}$ in the $(J_1, J_2, J_3)$-action plane. The energy-surfaces for arbitrary (negative) energies are simply given by scaling the action coordinates. Unfortunately, there is no

general procedure to derive the action integrals analytically. However, they can be calculated numerically as outlined, e.g., in Refs. 15) and 20). Locally (i.e., for $J_2 \gg J_1, J_3$), $J_1$ describes mainly the radial motion of the outer electron, $J_2$ the radial motion of the inner electron, and $J_3$ the bending degree of freedom.

In Fig. 3 we show the energy shell $E=-1$ for the collinear configuration $J_3 \equiv 0$ in the $J_1/J_2$ plane. For $J_1=0$ the dimension of the torus decreases by one (the tori collapse to the fixed point in Fig. 2) and $J_2$ takes the value of the fundamental PO. $J_1$ becomes singular as $J_2$ approaches $Z/\sqrt{-2E}=\sqrt{2}$. The singularity reflects the fact that the outer electron approaches a (single-particle) ionization threshold and thus accumulates an arbitrary amount of action. The diverging action near thresholds is a property of long-ranged attractive interactions and indicates the existence of infinitely many quantized (Rydberg) states below the thresholds.

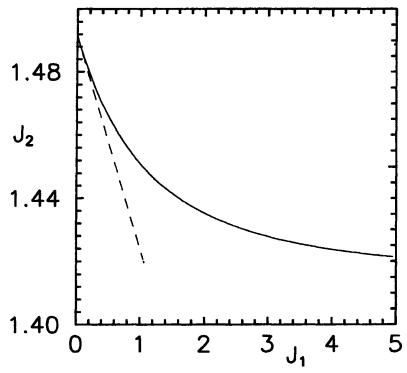


Fig. 3. Energy surrace $E=-1$ in the $J_1/J_2$-action plane for the collinear configuration with both electrons on the same side of the helium atom. The Gutzwiller approximation is drawn as a dashed line.

B. *The $e^-Z^{2+}e^-$ configuration*

Configurations where the electrons move on opposite sides of the nucleus are energetically favored because the electron-electron interaction is minimized. Quantum mechanically, these are the (resonant) states in which $\langle -\cos\Theta \rangle$ is close to unity. Here, $\Theta$ is the angle between $\boldsymbol{r}_1$ and $\boldsymbol{r}_2$. Such states are dominantly excited in single-photon transitions from the ground state.[21]

Equipotential lines for this type of collinear electron arrangement are shown in Fig. 4 together with a typical periodic trajectory. The system ionizes if either $r_1 \to \infty$ or $r_2 \to \infty$. As a matter of fact, the topology of the equipotential lines and of the boundary of the classically allowed region do not depend on the details of the underlying particle-particle interactions. The main characteristic of the potential surfaces is that there are two alternative ways of the system to ionize, i.e., only one particle (or equivalently one degree of freedom) can ionize whereas the other particle remains bounded. Similar potential

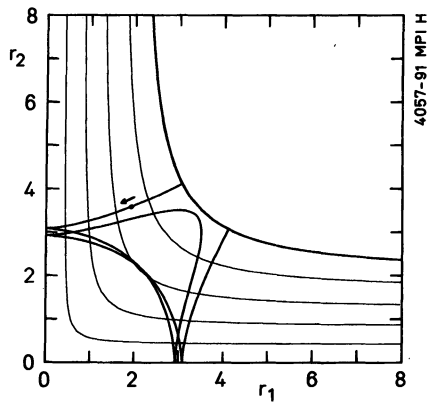


Fig. 4. Equipotential lines and boundary of the classical allowed region for the collinear electron configuration for helium with both electrons on opposite sides of the nucleus ($E=-1$). The PO $(+---)$ is also shown.

surfaces can be found in problems such as the hydrogen atom in a uniform magnetic field[22] (where the electron can ionize either parallel or anti-parallel to the magnetic field), the motion of triatomic molecules for energies below the three-particle breakup threshold,[23] the $x^2y^2$ potential,[24] or the motion of ballistic electrons in hetero junctions[25] modeled by elastic pinball scattering of particles (such as the four-disk scattering system[22] or the hyperbola billiard[26]).

The classical motion of the collinear helium atom with the electrons on different sides of the nucleus turns out to be fully chaotic, even though we cannot rigorously prove this. A system is called "chaotic" if all PO are linearly unstable and their number proliferates exponentially with the action (or some other length characteristic). The exponential proliferation becomes obvious if the PO can be mapped onto a tree of symbols as, e.g., for the anisotropic Kepler problem[4),27] or the diamagnetic Kepler problem.[22] The collinear motion of the helium atom suggests a binary coding for the PO.

To characterize the motion on the potential surface, Fig. 4, we introduce a symbolic description of the trajectories by recording the sequence $\{i_j\}$, ..., $i_{-1}$, $i_0$, $i_1$, $i_2$, ..., of electron collisions with the nucleus, i.e., $r_i=0$. Starting at the initial point indicated in Fig. 4 the PO is then coded by the periodically continued string of symbols $\cdots$12122121$\cdots$. Even though there is no restriction on allowed symbol sequences (*unrestricted symbolic dynamics*) it is convenient to redefine the code such that it reflects the discrete symmetries of the problem in a natural way. Here, the discrete symmetry corresponds to the exchange of electron coordinates $r_1 \leftrightarrow r_2$ (Pauli principle). Only an initial segment of a symmetric PO needs to be considered. An example for such a symmetric PO is the trajectory shown in Fig. 4. After some fraction of its period, the orbit will pass through an image (under the discrete symmetry group) of the initial point. The further evolution may then be obtained from symmetry images of the initial segment. This procedure is the classical pendant to the separation of discrete symmetries in quantum mechanics and to the symmetrization of the Green's function in the semiclassical theory.

For a redefinition of the coding scheme we consider the motion in the *fundamental domain*,[22),28] which is only half of the configuration space shown in Fig. 4 with an elastically reflecting wall at $r_1 \equiv r_2$. All information (either classically or quantum mechanically) is contained in the de-symmetrized motion of the fundamental domain,[29] to which we will restrict ourselves from now on. In the fundamental domain a collision is denoted by the symbol:

- $+$ when the previous collision was by the *same* electron, i.e., when the trajectory does not hit the $r_1 \equiv r_2$ boundary wall between two collisions,
- $-$ when the collision before was by the *other* electron, i.e., when the trajectory hits the $r_1 \equiv r_2$ boundary wall between two collisions.

Note that there can be at most one bounce between two crossings of the SOS which guarantees the uniqueness of the coding. Using this fundamental coding the symbol string for the PO reads $(+---)$. Now we have to add the *same* fundamental code (not the *image* 2121 of the initial segment 1212) to obtain the symbol string of the PO in the full domain, just as with the PO itself. The PO has (topological) length 4,

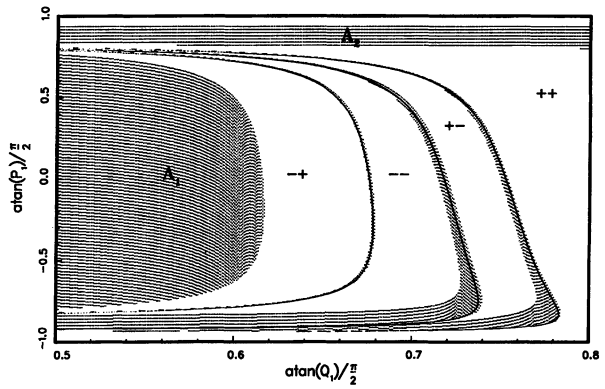


Fig. 5. Markov partition of the Poincaré surface of section $r_2=0$ with respect to regularized coordinates $Q_1=\sqrt{r_1}$, $P_1=2\sqrt{r_1}p_1$. The stable (collision) manifold (solid line) is surrounded by an ionization region (dotted area); the large areas labelled $A_1$ and $A_2$ belong to phase space points of trajectories for which the outer electron is ionized already at the first recurrence to the surface of section.

because its code consists of repetitions of a string of four symbols.

The triple collision for which all particle distances vanish plays a key role in understanding the existence of the symbolic dynamics. Normally, each phase space point uniquely defines a trajectory in the past and in the future. However, the equations of motion in the triple-collision singularity are non-regularizable, i.e., there exists a one parameter family of orbits starting or ending in the triple collision. They form a purely stable and unstable manifold, the so-called collision manifold.[30] The stable and unstable collision manifold tesselate the phase space and generate a Markov partition. This is demonstrated in the Poincaré surface of section for $r_2=0$ in Fig. 5. Each time the stable manifold crosses the Poincaré surface it divides the plane into $2^n$ distinct cells, where $n$ is the total number of intersections of the manifold with the surface. By reversal of time a similar structure is generated by the unstable manifold. (It is obtained by $p_1 \to -p_1$.) Figure 5 shows the first two intersections of the stable manifold with the SOS $r_2=0$.

The existence of the Markov partition guarantees the completeness of the symbolic dynamics, i.e., every binary code is represented by at least one trajectory. Again we label the different $2^n$ cells by a binary string of length $n$. Each cell contains a PO with precisely the same coding. To show the purely hyperbolic character of the system it would suffice to prove that the partitioning of phase space gets arbitrary fine in the limit $n \to \pm\infty$, i.e., that the volume of each Markov cell shrinks to zero. This is confirmed by numerical investigations, but, unfortunately, we do not know about any rigorous prove for this. Indeed, for the Positronium negative ion (which differs from the helium atom in that the 'nuclear' charge and mass are unity) the shortest PO of the collinear configuration is stable[31] and the corresponding Markov cell remains finite in the limit $n \to \pm\infty$.

For a *generating* Markov partition not only the volume of the cells but also the surfaces of the cells tend to zero. The intersections between the stable and unstable manifolds are then nowhere tangential. Orbits of marginal stability, i.e. with mono-

dromy matrix eigenvalues of unity,[29] are an indicator for tangential intersections of the manifolds. For the collinear configuration such a marginally stable PO with code (+) exists. It represents an ionized electron with zero kinetic energy at $r_1=\infty$, while the inner electron moves on a degenerated Kepler ellipse around the nucleus. The existence of this marginally stable orbit causes a cell with a finite surface in the Markov partition even though its volume shrinks to zero for arbitrary fine partitions.

The collinear $e^-Ze^-$ configuration represents an open system, i.e., one of the electrons can escape with an arbitrary amount of kinetic energy, while the other remains bounded to the nucleus. An ionization boundary cannot be defined in coordinate space since trajectories arbitrary far away can return to the nucleus. However, one can give an appropriate ionization criterium in phase space which is applicable at the outer turning point of the inner particle:[15] whenever $p_1>0$ at the outer turning point $p_2=0$ of the inner particle ($r_2<r_1$) the outer electron is ionized and will never return to the nucleus. In Fig. 5 the regions in the SOS are shown which fulfill the ionization criterium within two intersections with the surface of section. There are two big regions (labelled $A_1$ and $A_2$ in Fig. 5) belonging to trajectories which will

Table I. Various properties of the collinear periodic orbits of the helium atom. The action of a PO is given by $2\pi S/\sqrt{-E}$. $u$ is the stability exponent, i.e., the Liapunov exponent times the period of the orbit. The Morse index $\alpha$ for the motion in the symmetry plane and the winding number $\gamma$ for the linearised motion off the symmetry plane are given in the next columns. The type of fixed point (FX) is denoted by H for hyperbolic orbits and by IH for hyperbolic orbits with reflection (taken from Ref. 9)).

| No | Code | $S$ | $u$ | $\gamma$ | $\alpha$ | FX |
|---|---|---|---|---|---|---|
| 1 | + | 1.41421 | 0 | 0.5 | 2 | H |
| 2 | − | 1.82900 | 0.6012 | 0.5393 | 2 | IH |
| 3 | +− | 3.61825 | 1.8622 | 1.0918 | 4 | IH |
| 4 | ++− | 5.32615 | 3.4287 | 1.6402 | 6 | IH |
| 5 | +−− | 5.39452 | 1.8603 | 1.6117 | 6 | H |
| 6 | +++− | 6.96677 | 4.4378 | 2.1710 | 8 | IH |
| 7 | ++−− | 7.04134 | 2.3417 | 2.1327 | 8 | H |
| 8 | +−−− | 7.25849 | 3.1124 | 2.1705 | 8 | IH |
| 9 | ++++− | 8.56619 | 5.1100 | 2.6919 | 10 | IH |
| 10 | +++−− | 8.64307 | 2.7207 | 2.6478 | 10 | H |
| 11 | ++−+− | 8.93700 | 5.1563 | 2.7292 | 10 | H |
| 12 | ++−−− | 8.94619 | 4.5932 | 2.7173 | 10 | IH |
| 13 | +−+−− | 9.02690 | 4.1765 | 2.7140 | 10 | IH |
| 14 | +−−−− | 9.07179 | 3.3424 | 2.6989 | 10 | H |
| 15 | +++++− | 10.13874 | 5.6047 | 3.2073 | 12 | IH |
| 16 | ++++−− | 10.21674 | 3.0324 | 3.1594 | 12 | H |
| 17 | +++−+− | 10.57067 | 6.1393 | 3.2591 | 12 | H |
| 18 | +++−−− | 10.57629 | 5.6766 | 3.2495 | 12 | IH |
| 19 | ++−+−− | 10.70699 | 5.3252 | 3.2520 | 12 | IH |
| 20 | ++−−+− | 10.70699 | 5.3252 | 3.2520 | 12 | IH |
| 21 | ++−−−− | 10.74304 | 4.3317 | 3.2332 | 12 | H |
| 22 | +−+−−− | 10.87855 | 5.0002 | 3.2626 | 12 | H |
| 23 | +−−−−− | 10.91015 | 4.2408 | 3.2467 | 12 | IH |

ionize in a single step without participating in the chaotic dynamics. Most of these trajectories belong to the simple reaction $e^-+He^+ \to e^-+He^+$, when an incoming electron scatters without significant time delay in the inner region. This type of ionization occurs also when the electron-electron interaction is switched off.

A different ionization mechanism is related to the stable collision manifold which is surrounded by a layer of ionizing trajectories in the SOS. By time reversal there exists an equivalent mechanism to capture an electron from $r_1=\infty$ along the unstable manifold into the chaotic region near the triple-collision point. The existence of this type of ionization (or temporary capture) is related to the existence of the chaotic electron-pair motion and to the non-vanishing interaction between the electrons.

The collinear POs are now mapped onto strings of the binary symbols $\{+, -\}$. We have calculated all orbits up to symbol length 16 (8800 in number). Some properties of the 23 orbits up to symbol length 6 are listed in Table I: the scaled actions $S$, the eigenvalues of the stability matrix $\boldsymbol{M}$,[29] and some discrete properties of the POs. The coding automatically takes care of the discrete properties. The twist of the stable and unstable manifolds along the orbit (i.e., the maximal number of conjugate points within the collinear configuration) is given by the symbol length, and the Morse index $\alpha$ by twice the symbol length. The type of fixed point is determined whether the number of $(-)$ in the sequence is odd or even. All POs are unstable with respect to the motion inside the symmetry plane. However, nearly all of them are stable in the bending degree of freedom perpendicular to the symmetry plane. We also found some orbits which are unstable, but the instabilities are always very small compared to those in the symmetry plane.

## § 3. Quantum mechanical ab initio calculations

For not too highly doubly-excited states the spectrum of the helium atom for $\boldsymbol{L}=0$ can be characterized as follows. A set of $N$ different Rydberg series converges to each hydrogenic energy level $E=-2/N^2$ of the $He^+$ ion. This is drawn schematically in Fig. 6. The lowest Rydberg series of singly excited states $N=1$ contains bound states only. The states of all the other Rydberg series represent doubly-excited resonances which decay into the continua of the lower Rydberg series. The number of continuum channels increases quadratically with the excitation $N$ of the inner electron. As long as $N$ is small ($N<5$), Rydberg series converging to different thresholds do not overlap and the structure of the spectrum is rather

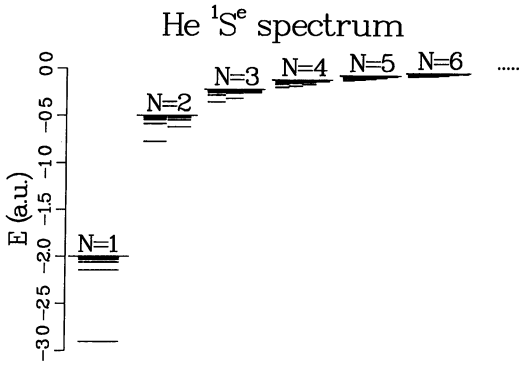


Fig. 6. Schematic view of the spectrum of the helium atom: $N$ different Rydberg series converge to the $N$-threshold of the $He^+$ ion. For each $N$ the energetically lowest (highest) series corresponds to configurations in which the electron-electron interaction is minimized (maximized), that is, to near-collinear configurations with both electrons being on different (the same) sides.

simple. For higher excitation of the inner electron the Rydberg series begin to overlap and the structure of the spectrum becomes more complicated.

To solve the Schrödinger equation associated with the Hamiltonian (1) numerically is a non-trivial problem for states in which both electrons are highly excited. Here we express the Schrödinger equation in the perimetric coordinates (2). In combination with Sturmian basis sets this allows an efficient representation of the Hamiltonian matrix.[32]

The total angular momentum $\boldsymbol{L}$ is conserved and its separation from the equations of motion reduces the number of degrees of freedom from six to four. Expressing the Jacobi coordinates $\boldsymbol{R}=\boldsymbol{r}_1-\boldsymbol{r}_2$, $\boldsymbol{r}=(\boldsymbol{r}_1+\boldsymbol{r}_2)/2$ in spherical $\boldsymbol{R}=(R, \Theta, \Psi)$ and cylindrical $\boldsymbol{r}=(\rho, \zeta, \varphi)$ coordinates respectively, the total two-electron wavefunction is given by

$$\psi_{LM}(\boldsymbol{r}, \boldsymbol{R})=\sum_{-L\leq m\leq L} D^{L*}_{Mm}(\Psi, \Theta, \varphi)\Phi_m(R, \rho, \zeta)\,. \tag{4}$$

The rigid top wavefunctions $D^L_{Mm}$ describe the overall rotation of the three-body complex and are eigenfunctions of $\boldsymbol{L}^2$ with eigenvalues $L(L+1)$ and eigenfunctions of $L_z$ with eigenvalues $M$ and $m$ in the space- and body-fixed frames, respectively. In the following we focus on states with $\boldsymbol{L}=0$. Then $L=M=m=0$ and the total spatial wavefunction reduces to (dropping the indices) $\psi(\boldsymbol{r}, \boldsymbol{R})=\Phi(R, \rho, \zeta)$. The disappearance of the rotational wavefunction $D^L_{Mm}$($D^0_{00}$ is a constant function) reflects the fact that the motion now takes place in a space-fixed plane.

The Hamiltonian is transformed into perimetric coordinates (for an explicit expression see, e.g., Ref. 33)) and expanded in a basis set of Sturmian functions.[32] One advantage of using perimetric coordinates in connection with a Sturmian basis is that the Hamiltonian matrix has a sparse banded structure. The unit matrix is also sparse and banded (but not diagonal). In addition, all non-zero matrix elements are of simple analytic form. This allows an efficient diagonalization in near-complete basis sets without using supercomputers.

Calculations of doubly-excited states requires the determination of the resonance parameters, i.e., the energies and the decay widths of the states. They are given by the real and imaginary part $E-i\Gamma/2$ of the eigenvalues of the complex rotated Hamiltonian $H(\theta)$ obtained by scaling $r_i\rightarrow r_i e^{i\theta}$ in (1). For sufficiently large $\theta$ these eigenvalues are independent of $\theta$ and the corresponding eigenfunctions are square integrable.[34]

The complex scaling transformation leads to a complex symmetric Hamilton matrix. We diagonalize the generalized eigenvalue problem using a Lanczos algorithm which takes advantage of the sparse matrix structures.[35] Typically, we use basis sets with up to 63 basis functions for each of the three degrees of freedom leading to matrix dimensions up to $\sim$22000. We then obtain resonance parameters within near-machine precision even for highly doubly excited states.[32] This allows us to check very accurately the predictions of the classical and semiclassical methods described in this review.

## § 4. Semiclassical quantization

### A. *Periodic orbit theory*

Using the relation between the density of states $\rho$ and the trace of Green's function $G$, $\rho(E)=-(1/\pi)\mathrm{Im}\,\mathrm{Tr}G$, Gutzwiller established a connection between the quantum eigenvalues and the classical PO of a Hamiltonian system.[4),36)] The semiclassical approximation of Feynman's path-integral formalism leads to a representation of the Green's function as a sum over classical paths. The stationary phase evaluation of the trace gives the response function $g_{\mathrm{scl}}$ (the imaginary part of which is the semiclassical level density) as a sum over classical POs. The response function $g_{\mathrm{scl}}=g_0+g_{\mathrm{osc}}$ is composed of a smooth part $g_0$ and of oscillatory contributions $g_{\mathrm{osc}}$. The smooth part contains information about the static, geometrical features of the Hamiltonian, e. g., the size of the energy shell determines the leading term in $\hbar$ of $g_0$. The oscillatory part contains the dynamical information and turns out to be a sum over all contributions $g_{\mathrm{ppo}}$ of the primitive (i.e., non-repeated) periodic orbits (PPO) and their multiple traversals (given by the index $r$)[4)]

$$g_{\mathrm{ppo}}=\frac{-i}{\hbar}\frac{dS_p}{dE}\sum_{r=1}^{\infty}\frac{e^{(iS_p/\hbar-i\alpha_p\pi/2)r}}{|\det(\boldsymbol{M}_p{}^r-1)|^{1/2}}\,. \tag{5}$$

The stability character of each PO determines its weight and therefore its significance for the spectrum. Particularly, in evaluating the sum over the PPO one has to distinguish between stable and unstable orbits and one has to treat them separately. As it turns out, the quantization of stable orbits represents an approximate EBK-quantization of the torus structure around the stable orbit, see § 4.B. The contributions of the unstable orbits representing the hyperbolic Hamiltonian flow have to be resummed as their combined contributions do not converge, see § 4.C.

### B. *Quantization of elliptic islands: the frozen planet configurations*

The frozen planet PO described in § 2.A is linearly stable in all dimensions. The two pairs of eigenvalues of the stability matrix $\boldsymbol{M}$ are then complex numbers on the unit circle, i. e., $\exp(\pm 2\pi i\gamma_R)$ and $\exp(\pm 2\pi i\gamma_\Theta)$. For trajectories close to the PO the frequency ratios of the radial and angular motion transverse to the PO are given by the winding numbers $\gamma_R=0.0677$ and $\gamma_\Theta=0.4616$, respectively. Expanding the determinant in (5) into geometric series, the contribution of the frozen planet PO to the density of states is

$$\rho\sim\sum_{r=1}^{\infty}\sum_{k,l=0}^{\infty}\exp\left[2\pi ir\left(\frac{\tilde{S}(E)}{\hbar}-\frac{\alpha}{4}-\left(l+\frac{1}{2}\right)\gamma_R-2\left(k+\frac{1}{2}\right)\gamma_\Theta\right)\right], \tag{6}$$

where the number of conjugate points along the trajectory is already contained in the winding numbers. The Morse index $\alpha=2$ comes from the singularities in the Green's function related to the vanishing velocity at the turning point of the electron pair motion and to the binary collision of the inner electron, for which the Jacobian of the transformation from (six-dimensional) Euclidian coordinates to an appropriate inter-

nal coordinate set (e.g. the perimetric coordinates (2)) vanishes.[36] The bending degree described by $(k, \gamma_\Theta)$ appears twice in the full three-dimensional problem (6) as there are two independent spatial directions for which bending can take place.

The sum over the repetitions $r$ in (6) is a geometric series which can be summed analytically. Thus Eq. (6) yields a triple-WKB formula with three quantum numbers $n, k, l$,

$$\tilde{S}(E)=2\pi\hbar\left(\left(n+\frac{1}{2}\right)+\left(l+\frac{1}{2}\right)\gamma_R+2\left(k+\frac{1}{2}\right)\gamma_\Theta\right). \tag{7}$$

Using the classical scaling property for the action and rearranging (7) results in a triple-Rydberg formula for the energies converging to the three-body breakup threshold,

$$E_{nkl}=-\frac{S^2}{\left(\left(n+\frac{1}{2}\right)+\left(l+\frac{1}{2}\right)\gamma_R+(2k+1)\gamma_\Theta\right)^2} \tag{8}$$

with $S=1.491499$ the scaled action of the PO. The semiclassical quantum numbers $n$, $k$ and $l$ reflect the separability of the associated semiclassical wave functions in local coordinates parallel and perpendicular to the PO. Nodal excitations along the orbit are described by $n$, whereas $k$ (bending motion) and $l$ (transverse radial motion) count the excitations perpendicular to the orbit.

For $^1S^e$ symmetry Table II summarizes the positions and widths of frozen planet resonances ($n$, $k=0$, $l=0$) with $n$ ranging from 2 to 15 for both the (exact) quantum and the semiclassical result using (8). Considering the rather large basis sets necessary to obtain the converged quantum results the accuracy of the semiclassical results

Table II. Energies $E_{nkl}$ and total decay widths $\Gamma/2$ for planetary states of $^1S^e$ symmetry and nodal quantum numbers $k=l=0$. The quantum energies are taken from a highly accurate compilation of doubly excited helium states.[51] The predictions of the semiclassical formula (8) are given as $E_{\mathrm{scl}}$.

| $n$ | $-E_{\mathrm{scl}}$ | $-E_{n00}$ | $\Gamma/2$ |
|---|---|---|---|
| 2 | 0.2479 2 | 0.2573 716 098 | 0.0000 105 640 |
| 3 | 0.1393 5 | 0.1410 641 562 | 0.0000 117 392 |
| 4 | 0.0891 45 | 0.0895 708 049 | 0.0000 020 241 |
| 5 | 0.0618 87 | 0.0620 535 586 | 0.0000 005 602 |
| 6 | 0.0454 58 | 0.0455 386 677 | 0.0000 002 024 |
| 7 | 0.0347 98 | 0.0348 426 426 | 0.0000 003 684 |
| 8 | 0.0274 91 | 0.0275 175 990 | 0.0000 011 841 |
| 9 | 0.0222 65 | 0.0222 845 888 | 0.0000 005 244 |
| 10 | 0.0184 00 | 0.0184 119 859 | 0.0000 000 582 |
| 11 | 0.0154 60 | 0.0154 682 592 | 0.0000 000 236 |
| 12 | 0.0131 72 | 0.0131 781 204 | 0.0000 000 228 |
| 13 | 0.0113 61 | 0.0113 614 424 | 0.0000 000 149 |
| 14 | 0.0098 930 | 0.0098 961 216 | 0.0000 000 052 |
| 15 | 0.0086 947 | 0.0086 970 578 | 0.0000 000 014 |

is rather impressive. It is hard to imagine that there is a more efficient description of the frozen planet states which would allow, similar to the semiclassical PO approach, the accurate quantization of this few-body problem on a pocket calculator.

In the derivation of the triple-WKB formula (7) we consistently expanded all expressions to leading order in $\hbar$. We then expect the absolute semiclassical error to be of the order $\hbar^2$ and the relative error to be of the order $\hbar/n$ (for $n \gg k, l$),

$$\tilde{S}(E_{nkl})/2\pi\hbar n \approx 1+\beta_{kl}\frac{\hbar}{n}, \tag{9}$$

which shows the semiclassical limit $\hbar \to 0$ to be equivalent to $n \to \infty$. In Fig. 7 we plot the quantum defect-like quantity $\mu_n$,

$$\mu_n = (S/\sqrt{-E_{n00}} - n) \xrightarrow{n\to\infty} (\gamma_R/2 + \gamma_\Theta^{+1/2}) = \mu_n^{\mathrm{scl}}. \tag{10}$$

From Fig. 7 we deduce the leading term of the semiclassical error in the quantum defect $\mu_n$ to be $\beta_{00} = -0.0366$. Thus the error is of the order of what we expected, but the prefactor $\beta$ is rather small.

Note that the triple-Rydberg formula (8) yields real energies. In the lowest semiclassical approximation presented here the wave functions are square integrable and represent exactly bound states. These states can autoionize semiclassically by dynamical tunneling,[37] but the decay widths for such processes decrease exponentially with the nodal excitation along the orbit. The formula applies to both symmetrical and antisymmetrical states of electron exchange (i. e., to the spectroscopic $^{2S+1}L^{\pi} = {}^1S^e$ and ${}^3S^e$ series). Again, dynamical tunneling lifts this doublet degeneracy and the exchange energies vanish exponentially in the quantum results,[32] but the precise determination of the splitting is beyond the scope of the lowest order semiclassical treatment.

In Fig. 8 we plot the widths of the resonances $(n, 0, 0)$ for both ${}^1S^e$ and ${}^3S^e$ symmetry on a logarithmic scale. Obviously, the total decay widths decrease exponentially even though they fluctuate rather largely around the general trend. The exponential stability of the quantum states is remarkable considering the vastly

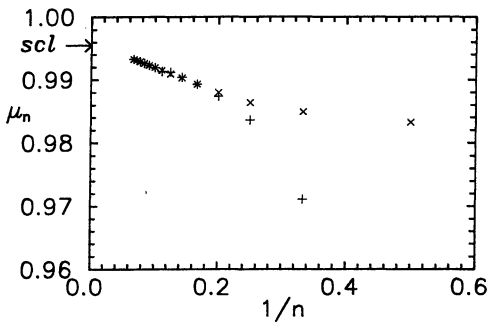


Fig. 7. Quantum defect $\mu_n$ as defined by Eq. (10). Both symmetry classes, ${}^1S^e(+)$ and ${}^3S^e(\times)$, are shown. The semiclassical limit $\mu_n^{\mathrm{scl}}$ is marked by an arrow.

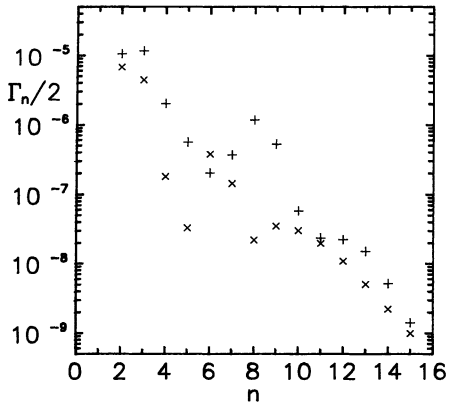


Fig. 8. Total decay widths $\Gamma/2$ of frozen planet states for both symmetry classes ${}^{1,3}S^e$.

increasing number of open channels into which the states can decay; the $(n, k, l) = (15, 0, 0)$ state, e.g., is coupled to 120 different continua. The extreme stability against (non-radiative) decay is a direct consequence of the semiclassical nature of these states.

A direct examination of the nodal structure of the associated wave functions is a more stringent test than comparing energy eigenvalues. Figure 9(a) depicts the conditional probability distribution of the wave function for the (6, 0, 0)-state for the collinear arrangement $r_{12}=r_1-r_2$. The off-collinear part of the probability density, not shown here, decreases exponentially indicating a zero-point motion in the bending degree of freedom. This zero-point motion is expressed by the assignment $k=0$. The coordinate $r_1(r_2)$ denotes the radial distance of the outer (inner) electron. The outer electron probability is strongly localized in the region $r_1 \approx 125$, reflecting the classical localization of the 'frozen' electron. Note also the large differences in the radial extents $r_i$. The nodal excitations are all directed along the frozen planet PO, which is a nearly straight line along the frozen-planet radius indicated by an arrow in the figure. Recalling the typical quadratic spacing of nodal lines in Coulombic systems, we achieve nearly constant nodal distances by using quadratically scaled axes as done in part (d). The number of nodes along the orbit is 6 in agreement with the semiclassical predictions. The wave function only has a zero-point distribution perpendicular to the orbit (in the symmetry plane of collinear motion), which agrees with the semiclassical local coordinate classification $(n, k, l)=(6, 0, 0)$.

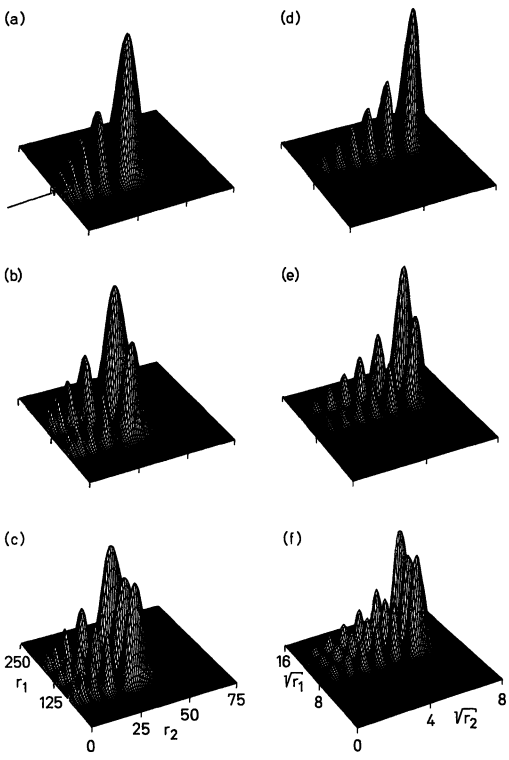


Fig. 9. Conditional probability densities of $(n, 0, l)$ frozen-planet states with $n=6$. The angle $\Theta$ between $r_1$ and $r_2$ is fixed to $\Theta=0$. The axes have a linear (left part) and a quadratic scale (right part), respectively. The states shown belong to $l=0$((a), (d)), $l=1$((b), (e)) and $l=2$((c), (f)). Only the parts $r_1>r_2$ are shown. The full wave function is symmetric in $r_1$ and $r_2$. The arrow in part (a) indicates the localization of the frozen-planet periodic orbit.

Wavefunctions with nodal excitations transverse to the orbit preserving the collinear character of the (quantum) motion are shown in parts (b), (e) and (c), (f) of Fig. 9. They correspond to the $l=1$ and $l=2$ nodal excitations of the $n=6$ manifold of states.

The triple-WKB formula (7) requires a non-symmetric treatment of the quantum numbers, $n \gg k, l$, as it represents a fixed point approximation of the Einstein-Brillouin-Keller (EBK) torus quantization. In the EBK quantization the Hamiltonian is transformed to action-angle variables and the different action integrals $J_i$ are

quantized separately. The quantized energy is then determined by the requirement that a trajectory accumulates the total action

$$J(E)=J_2+\gamma_1 J_1+\gamma_3 J_3 \tag{11}$$

after traversing a complete circuit 2 on the quantized torus defined by $J_i=2\pi\hbar(n_i+\alpha_i/4)$. The winding numbers $\gamma_i$ are the frequency ratios of the motion,

$$\frac{\partial H/\partial J_1}{\partial H/\partial J_2}=\frac{\omega_1}{\omega_2}=\gamma_1 . \tag{12}$$

The Gutzwiller approximation now consists in replacing the total action $J$ and the winding numbers $\gamma_i$ by their values at the PO $J_1=J_3=0$, hence it approximates the energy surface (11) by $J_2=S_{po}-\gamma_1^{po}J_1-\gamma_3^{po}J_3$. This is correct to leading order in $J_1$ and $J_3$, but may fail completely for large $J_1$, $J_3$. For the frozen-planet configurations and $J_3=0$ the fixed point approximation is plotted as dashed line in Fig. 3. Obviously, we cannot expect good results from this approximation for $J_1\gg J_2$. However, with the energy surface at hand, it is straightforward to quantize the action integrals $J_i$ separately. This has been done in Ref. 38) and some results are shown in Table III for the single-particle Rydberg series characterized by the set of quantum numbers $(J_2, J_3, J_1)=(n=7, k=0, l)$. Note that for $l\to\infty$ the energies now converge to the $N=n+1=8$ single-particle escape threshold of the $He^+$ ion. For the fixed point approximation (8) the limit $l\to\infty$, $n$ fixed, is beyond the range of its validity and it predicts convergence to the double-escape threshold $E=0$ instead.

The Rydberg series described above belongs to the blue edge (i.e. energetically highest) of the Rydberg series converging to the $N=8$ threshold, see Fig. 6. For larger values of $k$ Rydberg series $(n-k, k, l)$ converging to the same threshold are described. However, whereas the torus structure remains largely intact even for $J_1\to\infty$ the full stability island has only finite extent for $J_3$, i.e., for too large excitations $k$ of the bending degree of freedom the non-integrable part of the Hamiltonian, negligible for small $k\ll n$, becomes important and the electron pair motion may become chaotic. This is definitely the case near the red edge (i.e., the energetically lowest) of the Rydberg series in Fig. 6. The torus quantization must then be replaced by a different scheme, which will be the topic of the next section.

Table III. Energies for the doubly-excited Rydberg series $(n, k, l)=(7, 0, l)$ of frozen planet type. The quantum energies $E_l^{qm}$ are from Ref. 51), the semiclassical energies $E_l^{EBK}$ are obtained by quantizing the various action integrals. The relative semiclassical error $\varepsilon=|(E_l^{EBK}-E_l^{qm})/(E_\infty^{qm}-E_l^{qm})|$ is given in the last column (in percentage).

| $l$ | $E_l^{qm}$ | $E_l^{EBK}$ | $\varepsilon$ |
|---|---|---|---|
| 0 | 0.0348 426 | 0.0347 777 | 1.8 |
| 1 | 0.0343 124 | 0.0342 541 | 1.9 |
| 2 | 0.0338 901 | 0.0338 406 | 1.9 |
| 3 | 0.0335 489 | 0.0335 072 | 1.8 |
| 4 | 0.0332 682 | 0.0332 342 | 1.7 |
| 5 | 0.0330 357 | 0.0330 077 | 1.6 |
| 6 | 0.0328 414 | 0.0328 177 | 1.5 |
| 7 | 0.0326 753 | 0.0326 568 | 1.3 |
| 8 | 0.0325 329 | 0.0325 194 | 1.1 |
| $\infty$ | 0.0312 5 | 0.0312 5 | 0 |

### C. *Quantizing chaotic dynamics: —— Cycle expansion for near-collinear configurations of $e^-Z^{2+}e^-$ type ——*

The classical dynamics for collinear configurations with both electrons on different sides of the atoms turns out to

be fully chaotic (§ 2.B) and torus quantization cannot be applied. We now have to sum over the contributions (5) of *all* POs. This leads to the so-called Gutzwiller trace formula,

$$g(E)=\sum_n \frac{1}{E-E_n} \approx g_{\mathrm{scl}}(E)=g_0(E)+\sum_{\mathrm{ppo}} g_{\mathrm{ppo}}(E)\,. \tag{13}$$

It is convenient to rewrite the trace formula as a product over zeta functions.[39] Integration and exponentiation of Eq. (13) yields the spectral determinant for helium as an infinite product over zeta functions $\zeta_k^S$ of Selberg type,[9] which themselves are infinite products over so-called dynamical zeta functions $\zeta_{mk}$[40]

$$\prod_n (E-E_n) \sim \prod_{k=0}^{\infty} \zeta_k^S = \prod_{k=0}^{\infty} \prod_{m=0}^{\infty} \zeta_{km} = \prod_{k=0}^{\infty} \prod_{m=0}^{\infty} \prod_{\mathrm{ppo}} (1-t_{\mathrm{ppo}}^{(k,m)})\,. \tag{14}$$

The weight $t_{\mathrm{ppo}}^{(k,m)}$ of each PPO is given by ($z=1/\sqrt{-E}$)

$$t_{\mathrm{ppo}}^{(k,m)}=(\pm 1)^m \exp\left[2\pi i\left(zS-\frac{\alpha}{4}-2\left(k+\frac{1}{2}\right)\gamma\right)-\left(m+\frac{1}{2}\right)u\right], \tag{15}$$

where all classical quantities are given in Table I for the PPOs up to length 6. The plus sign applies to hyperbolic PPOs and the minus sign to hyperbolic PPOs with reflection.

The formal expression (14) relates the product over quantum eigenvalues with a product over PPO. The zeros of the Selberg-type zeta functions are the energy eigenvalues in the semiclassical approximation to Green's function traces. Unfortunately, the formal expression diverges in the region where the quantum zeros are located[41] and the zeros of the individual factors $(1-t_{\mathrm{ppo}}^{(k,m)})$ of the rhs cannot be identified with the zeros of the lhs. The lack of absolute convergence is well known for the Selberg and for the Riemann zeta function.[42),43] Resummation techniques must be used to obtain an analytic continuation of the zeta functions beyond their abscissas of absolute convergence.

We use the *cycle expansion*[28),40] to evaluate the semiclassical expression over PPOs. The idea of the cycle expansion is to expand the infinite product for the dynamical zeta functions $\zeta_{km}$ and to re-group it with respect to the total symbol length. For $\zeta_{00}$ this reads (dropping the indices $(k, m)$)

$$\prod_{\mathrm{ppo}} (1-t_{\mathrm{ppo}}) = 1-t_+-t_--[(t_{+-}-t_+t_-)]-[(t_{++-}-t_+t_{+-})-(t_{+--}-t_-t_{+-})]-\ldots\,. \tag{16}$$

Except for the fundamental orbits (+) and (−) each orbit contribution is accompanied by a compensating term pieced together from shorter orbits. Thus terminating the expansion at a given symbol length effectively means a re-summation of *all* orbits, with the approximation that the longer orbits are shadowed to increasing accuracy by the shorter ones. The absolute convergence of the re-grouped series (16) does of course not change. However, if each term $t_{ab}$ together with its shadowing term $t_at_b$ is viewed as a *single* entry $d_{ab}$ then the series (16) converges absolutely beyond the abscissa of absolute convergence of the full product. This is illustrated in Fig. 10 which shows the absolute values of the curvature terms $c_n=\sum_{(n)}|d_{(n)}|$ of symbol length $n$ for the zeta function $\zeta_{00}$ and $z=0$, i.e. for the semiclassical weights $t_{\mathrm{ppo}}$

$=\exp(-u/2)$. Also shown is the absolute sum of all terms of length $n$. Obviously, these coefficients diverge exponentially, whereas the regrouped curvature terms converge exponentially with a ratio $c_{n+1}/c_n \approx 0.65$. Thus the cycle expansion converges in the energy region close to the real axis where the resonances are located.

Similar to the treatment for the (doubly) stable frozen-planet orbit we identify $k$ as a semiclassical quantum number for the stable bending degree of freedom, i.e., the zeros of the individual zeta functions $\zeta_k^S$ are identical with the zeros of the full product.[44] In addition, the zeros of the Selberg-type zetafunctions $\zeta_k^S$ are identical with the zeros of the dynamical zeta functions $\zeta_{0k}$ except that $\zeta_{0k}$ has spurious zeros below some convergence limit $\mathcal{F}E<E_0<0$.[45]

In Table IV we tabulate the real part of the zeros for the cycle expansion of $\zeta_{00}$ for some resonances below the $N=4$ thresholds, i.e., for those Rydberg series which do not overlap energetically. We label the states by their 'independent-particle' quantum numbers $N$, $n \geq N$, which correspond to the principal quantum numbers of the electrons. For comparison the exact quantum energies of the energetically lowest Rydberg series converging to the $N$ thresholds are given. These states have only a zero-point motion for the bending degree of freedom and thus reflect the collinear character of these Rydberg series.

Generally, the energies obtained in the cycle expansion (as well as in the quantum mechanical calculations) are complex valued and we have only

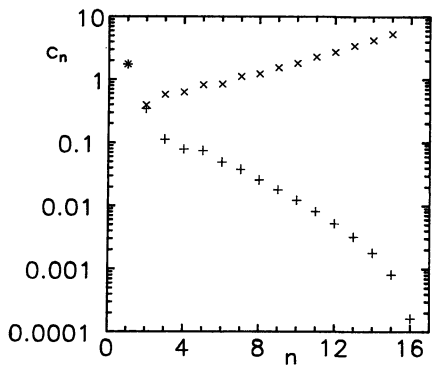


Fig. 10. Absolute values of the curvature terms $c_n$ of the cycle expanded product (+) and of the unexpanded product (×), see the text.

Table IV. Real part of the zeros of $\zeta_{00}$ obtained by cycle expansion of length $j$. The exact quantum energies are in the last column. The states are labelled by their principal quantum numbers. A dashed line as entry indicates a missing zero at that level of approximation.

| $N$ | $n$ | $j=1$ | $j=4$ | $j=8$ | $j=12$ | $j=16$ | $E_{qm}$ |
|---|---|---|---|---|---|---|---|
| 1 | 1 | 3.0984 | 2.9692 | 2.9001 | 2.9390 | 2.9248 | 2.9037 |
| 2 | 2 | 0.8044 | 0.7714 | 0.7744 | 0.7730 | 0.7727 | 0.7779 |
| 2 | 3 | — | 0.5698 | 0.5906 | 0.5916 | 0.5902 | 0.5899 |
| 2 | 4 | — | — | — | 0.5383 | 0.5429 | 0.5449 |
| 3 | 3 | 0.3622 | 0.3472 | 0.3543 | 0.3535 | 0.3503 | 0.3535 |
| 3 | 4 | — | — | 0.2812 | 0.2808 | 0.2808 | 0.2811 |
| 3 | 5 | — | — | 0.2550 | 0.2561 | 0.2559 | 0.2560 |
| 3 | 6 | — | — | — | 0.2416 | 0.2433 | 0.2438 |
| 4 | 4 | 0.2050 | 0.1962 | 0.1980 | 0.2004 | 0.2012 | 0.2010 |
| 4 | 5 | — | 0.1655 | 0.1650 | 0.1654 | 0.1657 | 0.1657 |
| 4 | 6 | — | — | 0.1508 | 0.1505 | 0.1507 | 0.1508 |
| 4 | 7 | — | — | 0.1413 | 0.1426 | 0.1426 | 0.1426 |

tabulated the real part of these energies. The widths of the resonances (i.e., the imaginary part of their energies) are still smaller than the semiclassical error in the real part and there is no likely reason why the imaginary part should be more accurate.

We find that the semiclassical cycle expansion works surprisingly good even for low excited states. The lowest state in each Rydberg series (the so-called intra-shell states of symmetric electron excitation) are already fairly described by truncating the expansion after the first term,[9),44)] i.e. by directly quantizing the fundamental orbit $(-)$[46)] which describes an asymmetric-stretch type motion of the electron pair. Inclusion of more and more orbits yields the higher excited states of the Rydberg series. One may wonder why the semiclassical analysis works fine even down to the ground state, which has a smooth and —more or less— structureless wave function. The reason is that the PO do not only contain the information about the underlying dynamics, but they also 'know' the size of the phase space. It is this property which often leads to rather good results when a fundamental (e.g., the shortest) orbit is naively quantized.

The helium spectrum becomes more complicated when Rydberg series converging to different $N$ thresholds overlap and states belonging to different series interfere. This happens for $N>4$, and in Table V we list the energies of resonances of the $N=6$ series which are perturbed by the lowest state belonging to the $N=7$ threshold. The perturbation of the states of the $N=6$ series becomes transparent by plotting their quantum defects $\mu_n$ which relate to their energies according to

$$-E=\frac{Z^2}{2N^2}+\frac{(Z-1)^2}{2(n-\mu_n)^2}\,. \tag{17}$$

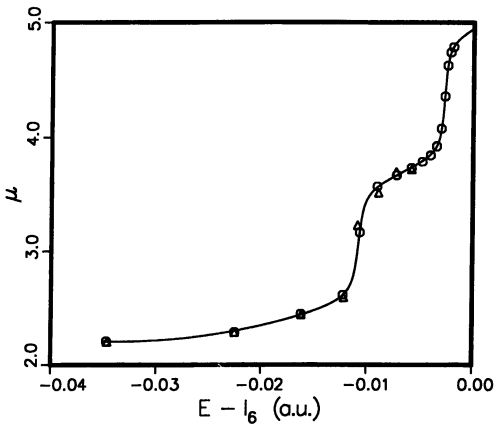


Fig. 11. Quantum defects $\mu$ (17) for the collinear states of the Rydberg series converging to the $N=6$ threshold, circles are quantum results, triangles are results obtained with the cycle expansion of length 16. The solid line represents a multi-channel quantum defect (MQDT) fit of the quantum results. The energies are plotted relative to the threshold energy $I_6=-2/6^2$.

For an unperturbed Rydberg series the quantum defect is a smooth and slowly varying function of the energy. An isolated perturber, however, causes a pseudo-resonant jump by unity of the quantum defect,[47)] that is, there is one more state in the Rydberg series over the range of the

Table V. Real part of the zeros of $\zeta_{00}$ obtained by cycle expansion of length 16. Energies of ab-initio quantum calculations for states between the $N=5$ and the $N=6$ threshold are taken from Ref. 51).

| $n$ | Cycle | quantum |
|---|---|---|
| 7 | 0.07802 | 0.07803 |
| 8 | 0.07172 | 0.07175 |
| 9 | 0.06772 | 0.06780 |
| 10 | 0.06645 | 0.06625 |
| 11 | 0.06447 | 0.06460 |
| 12 | 0.06281 | 0.06276 |
| 13 | 0.06136 | 0.06138 |

width of the perturber as one would expect without perturber. The quantum defects so obtained are shown in Fig. 11 for both the semiclassical and the quantum results. Obviously, the quantum defect increases by unity around $E-I_6=-0.011$. This pseudo-resonant jump of the quantum defect is caused by the lowest state of the Rydberg series converging against the $N=7$ threshold.[51] Thus the semiclassical cycle expansion is even able to reproduce such subtle effects as the interference of states on a rather small energy scale.

The semiclassical analysis also applies to the ${}^3S^e$ states, i.e., those which are anti-symmetric with respect to the exchange of particle (configuration space) coordinates. For the semiclassical Green's function we now have to take the Dirichlet boundary condition along the symmetry line $r_1 \equiv r_2$ instead of the von Neumann boundary condition. Thus each time a trajectory crosses the symmetry line, we have an additional phase loss of $\pi$. Again the coding takes care automatically of the additional total phase loss: each symbol '$-$' of the electron pair motion is associated with a crossing of the symmetry line. Results for this symmetry class can be found in Ref. 44).

## § 5. Summary and conclusions

At present, semiclassical theories undergo a rapid and exciting evolution. The present issue documents parts of this development, and we applied some of the semiclassical methods to a few-body problem, i.e., the two-electron helium atom.

The classical dynamics of the collinear helium atom with both electrons on the same side of the nucleus is fully stable. Torus quantization yields very accurate results for the positions of the associated quantum mechanical resonances. The semiclassical formalism also accounts semi-quantitatively for the decay widths and degeneracies of doublet states. The structure of the wave functions corresponds to what one would expect from considering the classical motion.

The classical dynamics of the collinear helium atom with both electrons on different sides is fully chaotic. An application of the Gutzwiller formula for the full three-dimensional problem combined with the cycle expansion yields a number of resonances with good accuracy. The interpretative ability of the methods illuminates the structure of the quantal motion. The analysis shows that the near-collinear intra-shell resonances are associated with the (fundamental) asymmetric stretch like motion of the electron pair. Semiclassically, this observation is nearly trivial. The result is nevertheless remarkable, in that it was widely believed that these resonances are associated with the in-phase symmetric stretch motion of the electron pair along the Wannier ridge.[48)~50)]

We are certainly at the beginning of refining the semiclassical methods for multi-dimensional methods like the PO-quantization approach. The torus quantization procedure for the frozen planet configurations represents a very efficient and accurate method to calculate eigenenergies. To a large extent this work can be done analytically and only a few trajectories have to be run numerically to obtain the energy shell in action space. On the other hand, the cycle-expansion method presented here to quantize the hyperbolic dynamics still lacks to be either efficient or being

highly accurate. Nevertheless, it is a first step in the right direction as it gives sense to the diverging Gutzwiller formula, the only semiclassical theory presently available for chaotic systems.

## Acknowledgements

This research was supported by the Deutsche Forschungsgemeinschaft (Wi877/2 and Wi877/5), and partly by the SFB 276 located in Freiburg. We are grateful to J. S. Briggs for his encouragement.

### References

1) M. S. Child, *Semiclassical Mechanics with Molecular Applications* (Clarendon, Oxford, 1991).
2) M. V. Berry and K. T. Mount, Rep. Prog. Phys. **35** (1972), 315.
3) J. H. Van Vleck, Philos. Mag. **44** (1922), 842.
4) M. C. Gutzwiller, *Chaos in Classical and Quantum Mechanics* (Springer, New York, 1990).
5) M. Born, *The Mechanics of the Atom* (Ungar, New York, 1927).
6) J. G. Leopold and I. C. Percival, J. of Phys. **B13** (1980), 1037.
7) K. Richter and D. Wintgen, J. of Phys. **B23** (1990), L197.
8) K. Richter and D. Wintgen, Phys. Rev. Lett. **65** (1990), 1965.
9) G. S. Ezra, K. Richter, G. Tanner and D. Wintgen, J. of Phys. **B24** (1991), L413.
10) J.-H. Kim and G. S. Ezra, in *Proc. Adriatico Conf. on Quantum Chaos*, ed. H. Cerdeira et al. (World Scientific, Singapore, 1991).
11) R. Blümel and W. P. Reinhardt, in *Directions in Chaos,* ed. B. L. Hao et al. (World Scientific, Hongkong, 1991), vol. 4.
12) B. Eckhardt, Preprint Universität Marburg; Habilitationsschrift, Universität Marburg (1991).
13) J. Müller, J. Burgdörfer and D. W. Noid, Phys. Rev. **A45** (1992), 1471.
14) P. Gaspard and S. A. Rice, Phys. Rev. **A48** (1993), 54.
15) K. Richter, G. Tanner and D. Wintgen, Phys. Rev. **A48** (1993), 4182.
16) C. Marchal, *The Three-Body Problem* (Elsevier, Amsterdam, 1990).
17) C. L. Siegel, Ann. Math. **42** (1941), 127.
18) H. M. James and A. S. Coolidge, Phys. Rev. **51** (1937), 857.
19) G. Wannier, Phys. Rev. **90** (1953), 817.
20) O. Bohigas, S. Tomsovic and D. Ullmo, Phys. Rep. **223** (1993), 45.
21) M. Domke, C. Xue, A. Puschmann, T. Mandel, E. Hudson, D. A. Shirley, G. Kaindl, C. H. Greene, H. R. Sadeghpour and H. Petersen, Phys. Rev. Lett. **66** (1991), 1306.
22) B. Eckhardt and D. Wintgen, J. of Phys. **B23** (1990), 355.
23) R. Schinke and V. Engel, J. Chem. Phys. **93** (1990), 3252.
24) P. Dahlqvist and G. Russberg, J. of Phys. **A24** (1991), 2736.
P. Dahlqvist, CHAOS **2** (1992), 43.
25) D. Weiss, K. Richter, A. Menschig, R. Bergmann, H. Schweizer, K. von Klitzing and G. Weimann, Phys. Rev. Lett. **70** (1993), 4118.
26) M. Sieber and F. Steiner, Phys. Lett. **A148** (1990), 415.
M. Sieber, Dissertation, Univ. Hamburg (1991).
27) G. Tanner and D. Wintgen, CHAOS **2** (1992), 53.
28) P. Cvitanović and B. Eckhardt, Phys. Rev. Lett. **63** (1989), 823.
29) B. Eckhardt and D. Wintgen, J. of Phys. **A24** (1991), 4335.
30) R. McGehee, Inventiones Math. **27** (1974), 191.
31) K. Richter, Dissertation, Univ. Freiburg (1991).
32) K. Richter and D. Wintgen, J. of Phys. **B24** (1991), L565.
K. Richter, J. S. Briggs, D. Wintgen and E. A. Solov'ev, J. of Phys. **B25** (1992), 3929.

33) Z. Zhen, Phys. Rev. **A41** (1990), 87.
34) Y. K. Ho, Phys. Rep. **99** (1983), 1.
35) D. Wintgen and D. Delande, J. of Phys. **B26** (1993), L399.
36) M. C. Gutzwiller, J. Math. Phys. **8** (1967), 1979; **10** (1969), 1004; **11** (1970), 1791; **12** (1971), 343.
37) M. J. Davies and E. J. Heller, J. Chem. Phys. **75** (1981), 246.
38) D. Wintgen and K. Richter, Comm. At. Mol. Phys. **29** (1994), 261.
39) A. Voros, J. of Phys. **A21** (1988), 685.
40) R. Artuso, E. Aurell and P. Cvitanović, Nonlinearity **3** (1990), 325, 361.
41) B. Eckhardt and E. Aurell, Europhys. Lett. **9** (1989), 509.
42) A. Selberg, J. Ind. Math. Soc. **20** (1953), 47.
43) J. Keating, *Proceedings of the International School of Physics "Enrico Fermi", Course CXIX*, ed. G. Casati, I. Guarneri and U. Smilansky (North-Holland, Amsterdam, 1993), p. 147.
44) D. Wintgen, K. Richter and G. Tanner, CHAOS **2** (1992), 19.
45) B. Eckhardt and G. Russberg, Phys. Rev. **E47** (1993), 1578.
46) We put the weight of the orbit (+) to zero as this orbit is not really existent. It describes an electron with zero kinetic energy infinitely far from the nucleus whereas the inner electron moves on degenerate Kepler ellipses, see, e.g. Ref. 15).
47) H. Friedrich, *Theoretical Atomic Physics* (Springer, New York, 1992).
48) U. Fano, Phys. Rep. **46** (1983), 97.
49) A. R. P. Rau, J. of Phys. **B16** (1983), L699.
50) S. Watanabe and C. D. Lin, Phys. Rev. **A34** (1986), 823.
51) A. Bürgers and D. Wintgen, to be published.